Building Tomorrow's Society
Bâtir la Société de Demain

Fredericton, Canada
June 13 – June 16, 2018/ *Juin 13 – Juin 16, 2018*

NUMERICAL MODELLING OF SLENDER SUPERELASTIC-SHAPE MEMORY ALLOY REINFORCED CONCRETE SHEAR WALLS

Morcos, Mena[1,3], Palermo, Dan[2]
[1] MASc Candidate, Department of Civil Engineering, York University, Toronto, Canada
[2] Associate Professor, Department of Civil Engineering, York University, Toronto, Canada
[3] mmorcos@yorku.ca

Abstract: A study is currently in progress to assess the self-centering capacity of Superelastic (SE)-Shape Memory Alloy (SMA) reinforced concrete slender shear walls. This study is based on numerical modeling to provide predictive assessments of the seismic behaviour and the ability to recover from imposed lateral displacements. Two ductile shear walls were constructed for future testing that will corroborate the nonlinear finite element analyses. The control wall was constructed with conventional deformed steel reinforcement in the longitudinal direction of the web and boundary zones, and in the transverse direction for shear reinforcement and buckling-prevention ties. A companion SE-SMA wall was constructed with similar reinforcing details, with the exception of replacing the conventional longitudinal steel reinforcement in the boundary zones with superelastic Nitinol SMA bars. The SMA bars were limited to the height of the plastic hinge region. Beyond the plastic hinge zone, the SMA bars were coupled to deformed steel reinforcement through mechanical couplers. The walls will be subjected to quasi-static load reversals, defined by a set of consecutive displacements, to failure. Axial loading is not imposed on the walls to reflect perimeter walls with low axial load. The focus of this paper is on preliminary nonlinear finite element analyses, which illustrates that the SMA reinforced wall provides approximately 61% displacement recovery; whereas the companion steel reinforced wall provides only 24% recovery after being subjected to 2.5% lateral drift. The damage predicted by the numerical model is substantially reduced in the SMA wall in comparison to the steel wall at similar levels of lateral displacement.

1 INTRODUCTION

Permanent damage within the plastic hinge regions promotes rotation of vertical structural elements leading to a series of interstory lateral drifts. A structure with a residual drift exceeding 2.5% is an indicator of both structural and non-structural damage and, thus, fails to be serviceable (Yazgan, 2010). In addition, this level of residual drift causes discomfort to occupants. A structure that has experienced notable residual drift is fated by the more feasible option between repair or demolition. However, the high cost associated with demolition and rebuilding is not economical, while repairing, if possible, may not rectify the deficiencies. As such, there is a need for the development of smart and more sustainable structures as alternatives that can reduce the probability of repairing or demolition.

Shape Memory Alloys (SMA), a smart material, offer self-centring solutions to structures, and a sustainable alternative to conventional steel reinforcement for concrete structures (Alam, 2007). Nitinol SMA – composed of approximately 56% nickel and 44% titanium – is available in a Superelastic (SE) or Shape Memory form. Superelasticity is achieved through the austenite material phase, which enables recovery from axial deformations when unloaded. Shape memory is retained when Nitinol is in the martensite material phase, or if work-strained beyond 6-8%, where recovery is only possible through the application

of heat (Ozbulut et al., 2011). Superelastic Nitinol is ideal for structural engineering applications owing to its self-centering capacity, dissipation of energy, and corrosion resistance (Menna et al., 2015). Previous experimental and numerical studies have demonstrated the wide array of applications of Nitinol for structural engineering. More recent research relevant to the study of self-centering slender concrete shear walls is the work of Saiidi and Wang (2006) on SE-SMA-reinforced bridge pier columns, and on SE-SMA-reinforced slender concrete shear walls by Abdulridha and Palermo (2017).

In this research program, predictive nonlinear finite element analysis is conducted on two ductile shear walls. The SMA-reinforced shear wall contains Ø12.7mm SMA bars as principle reinforcement within the boundaries of the plastic hinge zone only, using a non-invasive method of mechanical coupling to steel reinforcement. The second shear wall is constructed entirely using conventional steel reinforcement, to serve as a control point. This paper presents the results of a numerical finite element (FE) assessment, which illustrates the significant self-centering capacity and reduced damage experienced by the SE-SMA-reinforced slender concrete shear wall when subjected to lateral load reversals.

2 DEVELOPMENT OF SHEAR WALL MODELS

The basis for the design of the shear walls is the seismic provisions of CSA A23.3. Previous research (Abdulridha, 2013) established the dimensions for the slender shear walls of this study. The walls measure 1000mm in length and 2200mm in height (aspect ratio of 2.2), with a 150mm thickness across the web and boundary elements. The top of the wall is capped with a stiff 400mm x 400mm beam that measures 1600mm in length. The wall rests atop a stiff 500mm deep foundation block which measures 1600mm in length and 1000mm in width. Figure 1 illustrates reinforcement details for the SE-SMA reinforced wall.

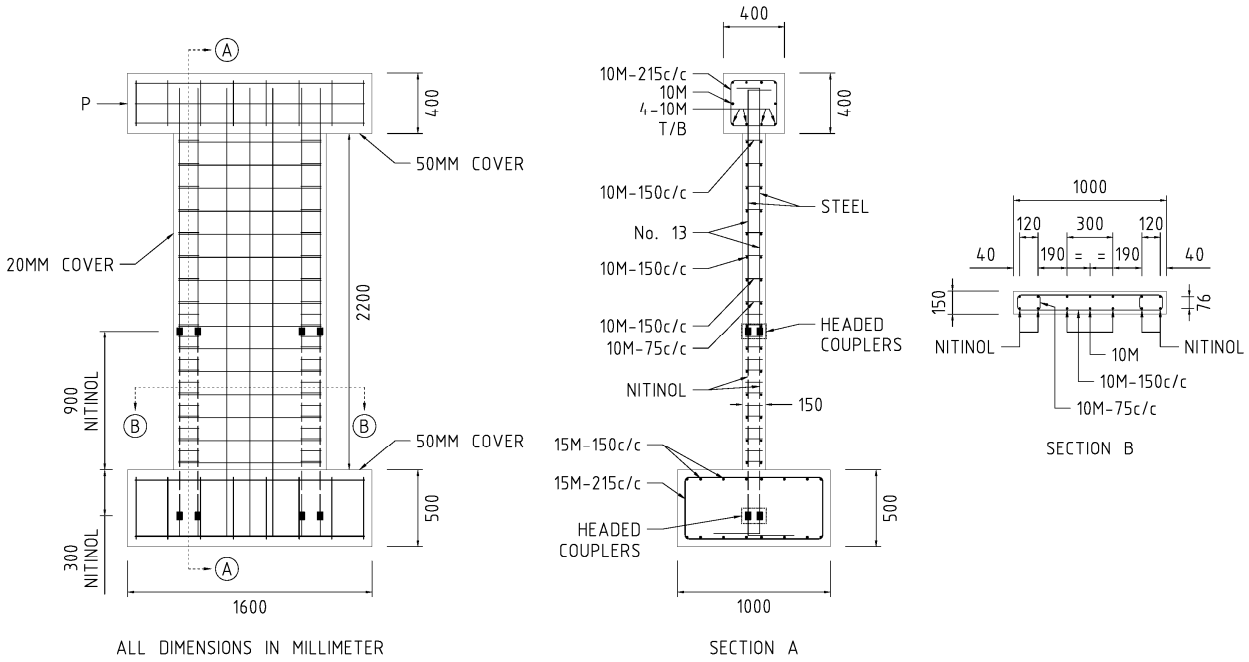

Figure 1. Reinforcement details of SE-SMA-reinforced wall.

To investigate the self-centering capacity of SE-SMA reinforcement, two slender shear wall specimens were constructed. A control wall was constructed with conventional deformed steel reinforcement in the longitudinal direction of the web and boundary zones, and in the transverse direction for shear reinforcement and buckling-prevention ties. Each boundary contains four 10M longitudinal bars, and the web has a total of six evenly spaced 10M longitudinal bars. A companion SE-SMA wall was constructed with similar reinforcement details, however, the conventional longitudinal steel reinforcement in the boundary zones is replaced with SE-SMA, as illustrated in Figure 1. The SMA bars were limited to 900mm within the height of the plastic hinge region; and extended 300mm into the foundation block. Each end of

the SMA bars is coupled to deformed steel reinforcement through a mechanical coupler. The SMA are smooth bars with a diameter of 12.7mm.

The results of experimental testing by Abdulridha (2013) indicated that the height of the plastic hinge region is approximately equal to the length of the wall. This study assumes the plastic hinge region of both walls extends 1000mm above the base, equal to the length of the wall.

3 EXPERIMENTAL PROGRAM

The shear walls are named SW-S and SW-N, where 'S' denotes steel-reinforced, and 'N' denotes Nitinol-reinforced. Figure 2 provides a photo of the walls after casting.

Figure 2. Walls after casting: SW-S (behind), SW-N (forward).

The steel-reinforced wall was constructed first. The construction was completed in two stages. First, the foundation block was poured, containing a reinforcing cage consisting of 15M deformed steel bars. The two 10M longitudinal reinforcing curtains for the boundaries and the web sections of the wall were embedded 400mm within the foundation symmetrically along the length. Second, the wall and cap beam were cast monolithically. The shear reinforcement and buckling-prevention ties were added to the wall prior to assembly of the formwork. The reinforcing cage of the cap beam consisted of 10M deformed steel bars. The longitudinal reinforcement within the wall extend 300mm into the cap beam.

The construction of the SMA-reinforced wall was staged in the same manner. The SMA bars were coupled to deformed steel bars using confining mechanical couplers. This coupling system does not pinch or gouge when forming a grip, as common with screw-lock coupling systems, which locally reduce the cross-section of reinforcement. The confining coupler utilizes a forging process to form an inversed conical head at the ends of reinforcing bars, which are then secured against each other using wedge action when the male and female components of the coupler are torqued together (Figure 3).

Figure 3. Mechanical couplers with headed deformed steel bar and headed SMA bar.

After demoulding the steel-reinforced wall, it was observed that some regions along the base were poorly consolidated. The most severe honeycombing was along each boundary, spanning about 200mm in length and 150mm in height and penetrating about 35mm of the wall thickness from each side. The honeycombing spread lightly along the web at the base, spanning 400mm in length and 100mm in height, penetrating 20mm from each side. The honeycombed regions at the boundaries were removed through the complete depth of the wall. The regions across the web were chipped to a depth of 25mm on each side. Self-Consolidating Concrete (SCC) was used to repair the removed concrete as illustrated in Figure 4. The steel-reinforced wall was renamed to SW-S(R); the '(R)' denotes the repair.

Figure 4. Repaired steel-reinforced wall.

Both specimens will be tested under quasi-static load reversals to simulate the effects of a seismic event. Each wall was constructed with six perforations in the foundation block that will be anchored to the strong floor of the laboratory using 2-1/2 in. diameter threaded rods. The cap beam is fitted with four PVC conduits to allow for passage of four 1 in. diameter threaded rods to connect to the head of a hydraulic actuator, which is mounted horizontally to the strong wall. During testing, the walls will be laterally supported to prevent twisting.

Each wall will be monitored by 32 strain gauges on the reinforcing steel and 14 instruments, a combination of linear and cable potentiometers. The strain gauges in SW-S(R) are rated for up to 2% strain. The strain gauges monitoring the SMA bars in SW-N are rated for post-yield strains up to 15 to 20%. The deformed steel reinforcement in SW-N is monitored with the same strain gauges as in SW-S(R).

4 FINITE ELEMENT MODELING AND ANALYSIS

Program VecTor2 was used in this study to conduct nonlinear analysis of the walls. A total of ten materials were used to define the constitutive models – three concrete mixes, and six reinforcement types, plus the coupler. The material properties were obtained by testing samples taken from the same materials used to construct the walls. Table 1 lists the properties of the concrete mixes. The reinforcement used to construct SW-S [SW-S(R)] include 15M bars (Ø = 16mm, F_y = 472.5MPa, F_u = 578MPa) for the foundation block, and 10M bars (Ø = 11.3mm, F_y = 454.4MPa, F_u = 570MPa) for the wall and the cap beam. The foundation block of SW-N was constructed of the same 15M steel reinforcement. The steel reinforcement used for the wall and cap beam, sourced from other suppliers, include 10M bars (Ø = 11.3mm, F_y = 529.4MPa, F_u = 686.5MPa), and #13 bars (Ø = 12.7mm, F_y = 474.5MPa, F_u = 639.5MPa). The properties of the 12.7mm-diamter SMA bars, based on the manufacturer, are F_y = 380MPa and F_u = 900MPa, while the mechanical couplers have a diameter of 35mm, with F_y = 690MPa and F_u = 795MPa.

Table 1: Concrete Material Properties

Wall	Type	$f`_c$ (MPa)	Aggregate Size (mm)
SW-S & SW-S(R)	30MPa Normal Concrete	47.2	14
	Sika Sikacrete-08 SCC	57.3	8
SW-N	30MPa Normal Concrete	36.9	14

The default constitutive models for the concrete and deformed reinforcing steel within VecTor2 were selected for this study. The SMA model was based on the work of Abdulridha et al. (2012) as illustrated in Figure 5. The SMA constitutive model captures plastic offsets in the unloading stage.

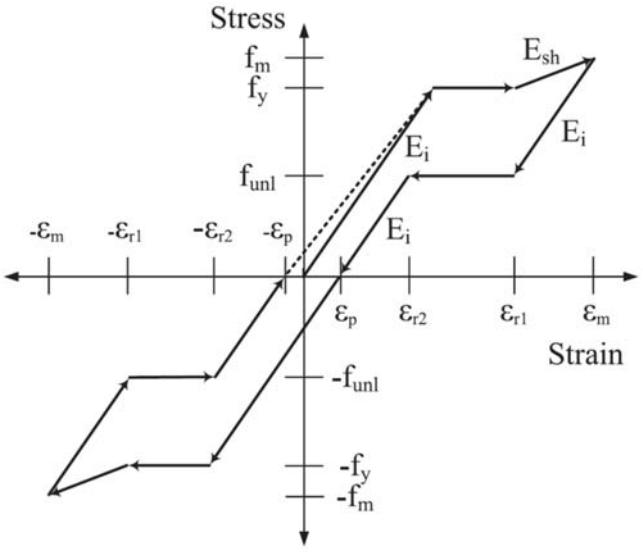

Figure 5. Superelastic Nitinol constitutive model for finite element analysis – plastic offset model (Abdulridha et al., 2012).

This model depicts the behavior of SE-SMA through a series of linear branches through loading and unloading. Loading along the strain hardening path captures the phase transformation from austenite to detwinned martensite. Unloading along the strain recovery phase exhibits the superelasticity and deformation recoverability of Nitinol. This model captures residual plastic deformations formed as the martensitic Nitinol begins to strain harden beyond 6 to 8% strain.

Three finite element models were developed: SW-S, SW-S(R), and SW-N. The steel-reinforced wall model SW-S was assessed to represent the intended condition of the wall and to serve as a benchmark for the repaired wall. The repaired steel-reinforced wall model SW-S(R) was assessed to determine the performance of the structure in its current condition. The SMA-reinforced wall model SW-N was assessed to determine the self-centering capacity in comparison to the control wall.

In a previous study (Abdulridha 2013), the wall models were discretized using element sizes of 100mm x 100mm. The FE models redeveloped for this study have four times the resolution of the previous models, composed of a mesh with predominantly 50mm x 50mm elements. The finer mesh is expected to better capture the bond-slip interaction between the smooth SMA bars and concrete.

Each model is similar, with five distinct regions as illustrated in Figure 6. The discretized concrete regions are the web, top and bottom boundaries, concrete cover, and stiff elements (cap beam and foundation block). The web region, of the steel-reinforced model, has a reinforcement ratio 0.89% in the transverse direction accounting for the shear reinforcement. In the boundaries, within the plastic hinge region, shear reinforcement and buckling-prevention ties are defined by a transverse ratio of 2.67%, and an out-of-plane ratio of 1.85%. The boundaries, above the plastic hinge region, have similar reinforcement with reduced ratios of 1.78%, and 1.11% for the transverse and out-of-plane directions, respectively. The concrete cover regions are unreinforced. All transverse reinforcement is modelled as smeared within the concrete elements. The SMA-reinforced wall has identical attributes of smeared reinforcement.

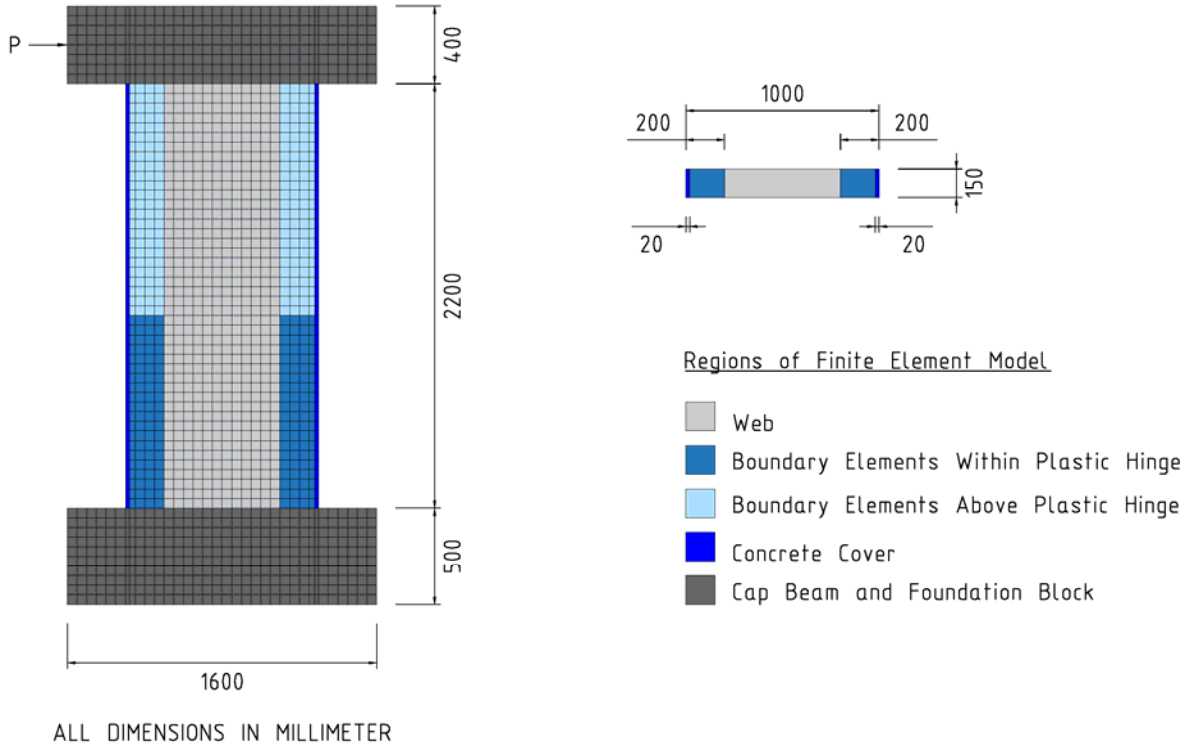

Figure 6. Typical discretization of concrete elements in wall model.

The mesh of the foundation block and cap beam conformed to the aspect ratios and dimensions of the wall, primarily starting at a ratio of 1:1 for the web, fixing elements to dimensions of 50mm x 50mm. The meshing of the boundary elements maintained a 1:1 aspect ratio, except for a 2.5 ratio to capture a 20mm concrete cover, and the elements adjacent to the cover and typical boundary elements that were 30mm x 50mm.

In SW-S, SW-S(R), and SW-N, the longitudinal reinforcement was modelled with truss elements that originated at 100mm from the top of the cap beam and extended to 100mm above the base of the foundation block. The longitudinal reinforcement in the web is spaced at 150mm on centres, while in boundary elements the reinforcement is spaced at 120mm. Truss elements representing deformed steel reinforcement are assumed to be perfectly bonded to the concrete elements. In the SW-N model, link elements simulate the bond between the SMA truss elements and the concrete elements. The bond behaviour of the link elements is governed by the Eligehausen bond model. Within the boundaries of the plastic hinge zone, the truss-elements representing the mechanical couplers are located at 900mm above the base of the wall, and are 50mm long. The same type of truss-element is located 300mm below the base of the wall into the foundation block below each boundary.

In the repair model, the SCC material is introduced as new regions depending on thickness. At the bottom of the boundaries, new regions are formed with the thickness of the wall; similarly, for the concrete cover at each end of the wall. Where poor consolidation did not completely penetrate the thickness of the wall, the SCC material is applied in 25mm thick layers on each side of the web. Between the layers of SCC across the web is a 100mm thick layer of the original concrete.

Each wall model was loaded laterally at an elevation of 2400mm from the base of the wall, through the centre of the cap beam, for uniform distribution of the lateral load. The calculated drifts are relative to this elevation. Pushover analyses were conducted to approximate an initial yield displacement for each wall according to the method by Park (1989). The approximated yield displacements are 12mm for SW-S and SW-S(R), and 32mm for SW-N. The greater yield displacement for SW-N is attributed to a reduced stiffness in the wall due to the use of SMA in the boundaries. At yielding of SW-N, a major flexural crack along the base developed, the longitudinal reinforcement in the web yielded, the onset of yielding of SMA

reinforcement in the tension boundary zone initiated, and cover loss in the compression boundary was evident. For the purpose of imposing a similar loading protocol, the yield displacement for both walls was assumed to be 12mm. [Note that the displacement intervals defining the loading cycles, are multiples of the yield displacement, according to ATC-24 (1992)]. The initial cycles targeted one-sixth, followed by one-third, then one-half of the yield displacement. Beyond the yield displacement, the displacement intervals were increased by one-half the yield displacement until attaining four and a half times the yield displacement. Three repetitions were imposed at each loading cycle up to this displacement level. Thereafter, two repetitions were used at five and seven times the yield displacement. Loading was terminated at a displacement of 84mm (3.5% drift). It was predetermined that loading would not exceed this displacement level to permit repairing.

5 RESULTS

The results from the pushover analyses predicted yielding at 31.3mm of displacement under a lateral load of 140kN, and a peak lateral load of 196kN at a displacement of 235mm for SW-N. The wall experienced an ultimate displacement of 252mm at a lateral load of 157kN. In comparison SW-S(R) yielded at 11.3mm at 130kN of lateral load, with a peak capacity of 163kN at 288mm of lateral displacement. SW-S(R) attained an ultimate displacement of 303mm corresponding to 130kN of lateral load. The model for Wall SW-S provided similar results as the model for Wall SW-S(R). Figure 7 provides the lateral load-displacement responses for the wall models.

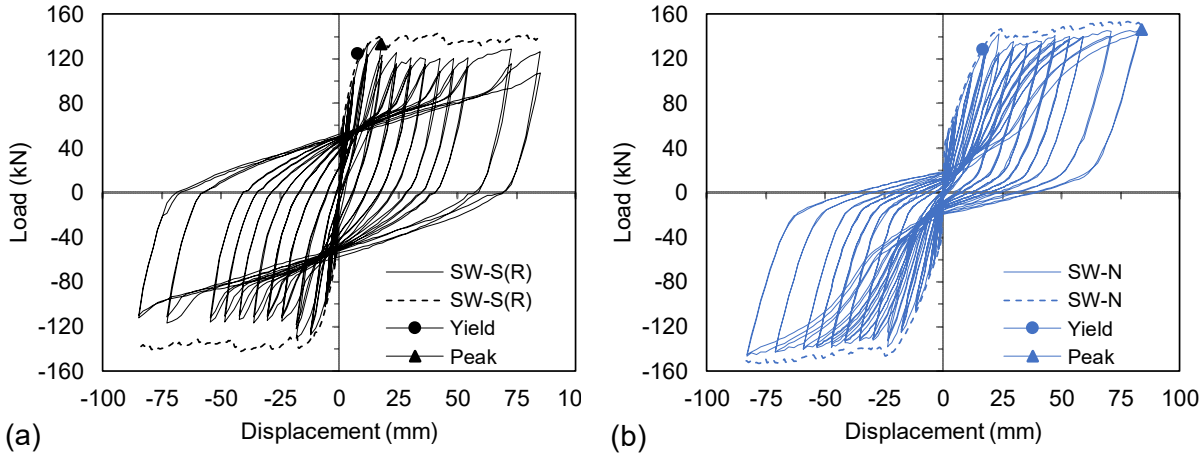

Figure 7. Lateral load-displacement responses: (a) Wall SW-S(R); and (b) Wall SW-N.

The yield point and peak load of each wall was based on the average of the positive and negative directions. The SW-N model yielded at a displacement of 17mm corresponding to a lateral load of 127.7kN, and experienced a peak capacity of 146.5kN at a displacement of 84mm. The SW-S(R) model yielded at approximately 7.8mm at a lateral load of 124kN. The peak lateral capacity was 133kN at 17.8mm of displacement. This behaviour is attributed to yielding of the longitudinal steel reinforcing bars in the boundaries and the web. Strain hardening was observed to develop gradually beyond 72mm of lateral displacement. The hysteretic responses of SW-S and SW-S(R) were similar, indicating a negligible impact of the repair on the performance of the steel-reinforced wall.

The larger yield displacement of SW-N is attributed to the lower modulus of elasticity of Nitinol bars. It is observed in the numerical models that the longitudinal steel in the web of SW-N yields while the SMA bars are below the strain recovery limit of 6%. This is demonstrated in the hysteretic response as a softening of the wall, and an elongation of the global yield point to a larger lateral displacement. Comparatively, SW-S(R) exhibits a stiffer behaviour due to the higher modulus of elasticity of the steel reinforcement in the boundaries. Abdulridha and Palermo (2017) suggested, that in such cases, a comparison of drift capacity is an adequate measure.

The lateral load-displacement responses of SW-S(R) and SW-S are very similar with wide hysteretic loops that are maintained with increasing lateral displacement. The steel-reinforced wall was able to recover lateral displacements only to the end of the 6mm loading cycle. The hysteretic response of SW-N exhibits pinching, which is attributed to the recoverability of the SMA bars upon unloading. Full recovery of lateral displacements was observed to the end of the 18mm loading cycle. Plastic deformations accumulated beyond the full recovery displacements stated above, however, SW-N exhibited substantial greater recovery than SW-S(R) at higher displacements. The high recoverability from lateral displacements provided by SW-N is indicative of the ability to self-centre, which is due to the superelasticity of SMA bars. The envelope of the lateral load-displacement responses and secant stiffness degradation are provided in Figure 8.

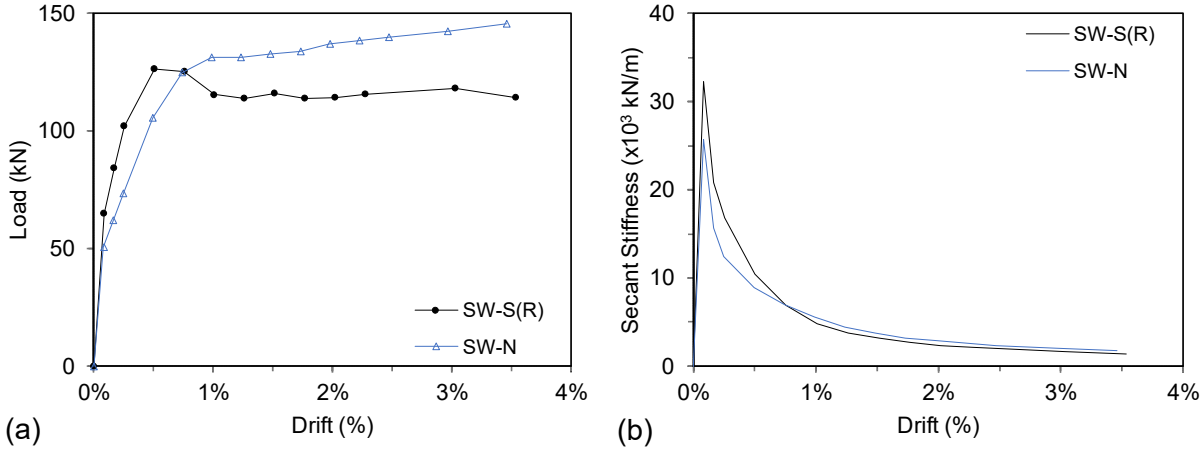

Figure 8. (a) Lateral load-drift envelope responses; and (b) Stiffness-drift degradation.

In SW-S(R), the lateral load capacity peaks at a low drift and then experiences an 8.7% reduction, which is maintained for the duration of loading. Conversely, SW-N experiences a gradual increase in load beyond yielding. In Figure 8(b), the stiffness of each wall peaks at 0.083% drift (2mm displacement), with a 25.6% increase in SW-S(R) relative to SW-N. Beyond this drift level, the stiffness experiences a notable degradation with increasing drift. At 0.75% drift (18mm displacement), the walls provide a similar secant stiffness, beyond which, the stiffness in SW-N exceeds the stiffness in SW-S(R). At 2.5% drift (60mm displacement) SW-N exhibits a 19.7% increase in stiffness over SW-S(R).

The predicted crack patterns are shown in Figure 9(a) and (b), while the energy dissipated by the walls is illustrated in Figure 9(c). At 2.5% drift, SW-S(R) experienced damage within the plastic hinge zone (Figure 9(a)), in the form of wide spread cracking. Both shear and flexural cracking are evident. The SW-N model (Figure 9(b)), predicted slight difference in the cracking pattern. Cracking at the base is predominantly horizontal. This is the result of the poor bond between the smooth SMA bars and the concrete.

The SMA-reinforced wall dissipates 29.5% less energy than SW-S(R) at the peak displacement (3.5% drift). The recovery action of the SMA bars causes a pinching of the hysteresis loops and a reduction in the calculated energy dissipation.

Damage in each wall initiated with flexural cracks followed by shear cracking in the web section of the wall. The large yield strain of the SMA bars in the boundaries of SW-N resulted in yielding first of the longitudinal steel reinforcement in the web of SW-N at 12mm of displacement. Yielding in the SMA initiated at 18mm of displacement. Yielding of the steel longitudinal reinforcement was initiated in the boundaries of SW-S(R) at 24mm of displacement. Each wall developed a major flexural crack along the base, which played a significant role in the behaviour. The SCC, located at the base, in SW-S(R) experienced crushing at 54mm of displacement (2.25% drift). Concrete crushing was not observed in SW-N up to 3.5% drift. Rupturing of the reinforcement was not observed in any of the walls due to limiting the analysis to 3.5% drift.

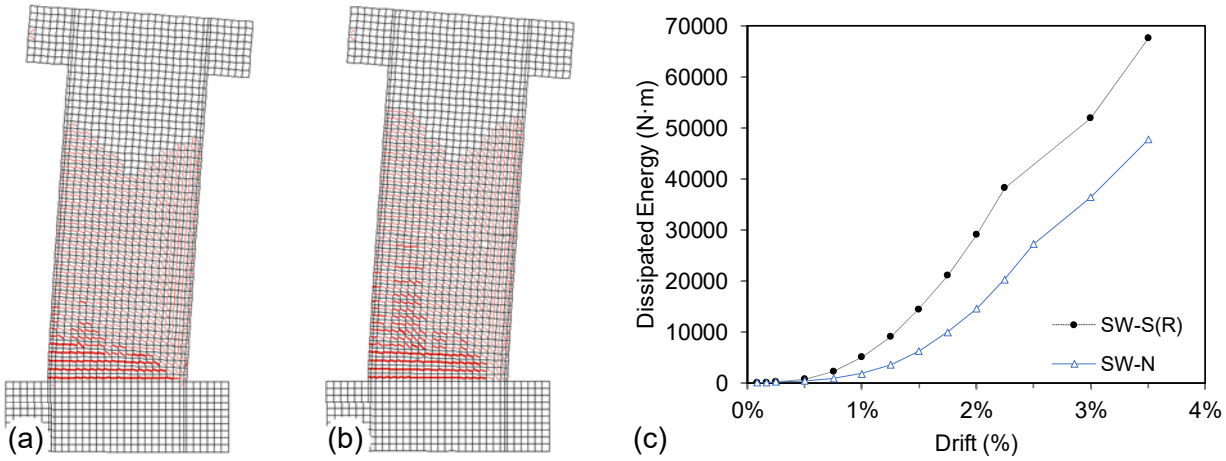

Figure 9. (a) SW-S(R) crack pattern at 2.5% drift; (b) SW-N crack pattern at 2.5% drift; and (c) energy dissipation.

6 DISCUSSION OF RESULTS

The self-centering capacity of a structure is a smart feature that can be achieved by using smart materials like SE-SMA. Figure 10 illustrates the recoverability of each wall against the probability of demolition due to excessive residual drift as developed by Ramirez and Miranda (2012). At 2.5% drift, SW-N recovered 61% of the imposed lateral displacement, while SW-S(R) recovered only 24%. This translates into a 0.98% residual drift for SW-N, which equates to less than a 10% probability of demolition. In comparison, SW-S(R) experienced a residual drift of 1.9%, yielding approximately 80% probability of demolition. Table 2 lists the residual drifts induced on each wall at the peak displacement of 84mm (3.5% drift). Although SE-Nitinol is more costly than traditional deformed steel reinforcement, it could provide substantial savings over the lifetime of a structure, specifically in zones with high seismic activity.

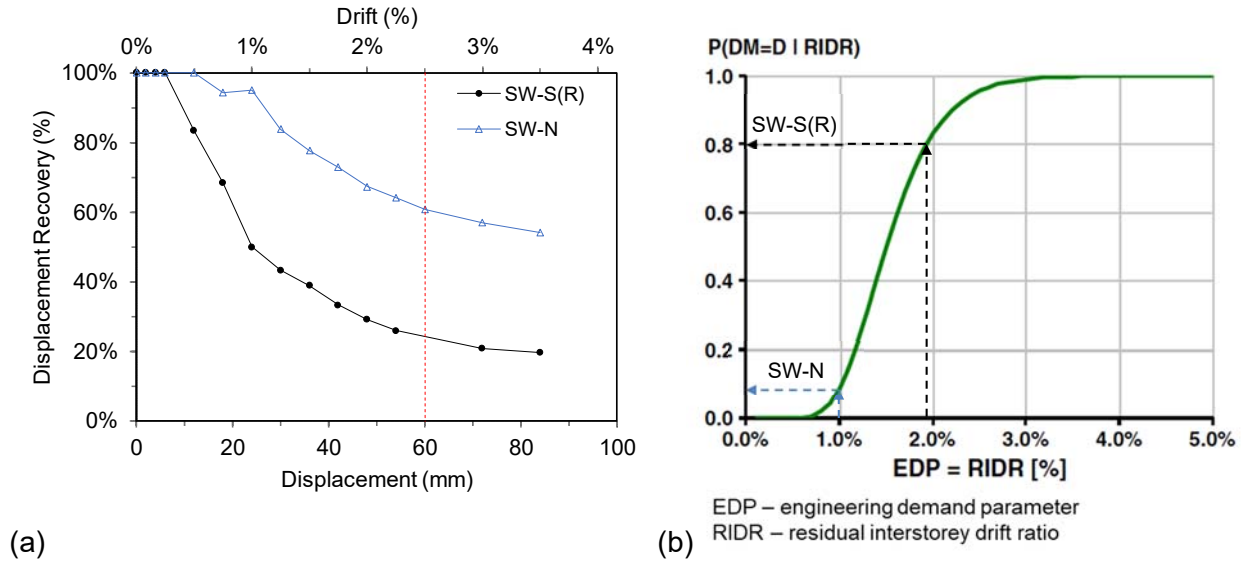

Figure 10. (a) Displacement recovery capacity of walls; (b) probability of demolition due to residual drift (Ramirez, C.M. and Miranda, E., 2012).

Table 2: Drift Recovery and Residual Capacity

Wall	Peak Displacement (mm)	Recovery (%)	Residual Drift (%)
SW-S	84	18.4	3.1
SW-S(R)	84	19.6	3.1
SW-N	84	54.2	1.8

7 CONCLUSIONS

This study focused on the self-centering capacity of slender reinforced concrete shear walls. To date, a slender concrete shear wall with SE-Nitinol reinforcing bars in the boundaries was constructed, along with a conventionally steel-reinforced control shear wall. Complimentary predictive numerical models were developed to assess seismic performance parameters under lateral load reversals. The following conclusions are drawn from the numerical study presented herein:

1. The initial high cost of SMA is significantly offset by the capacity to provide a self-centering mechanism to a structure. The SMA-reinforced wall presented in this study sustained less than 1% residual drift after being subjected to a lateral displacement corresponding to 2.5%.
2. The SMA wall reduced the probability of demolition by 70% in comparison to the companion steel-reinforced wall if considering a maximum imposed drift of 2.5%.
3. The extent of damage within the plastic hinge region was reduced in the SMA wall. A major horizontal crack develops along the base of the wall, which can be readily repaired.
4. The SMA wall dissipates approximately 63% of the energy dissipated by SW-S(R) at 2.5% drift. Furthermore, the SMA wall recovered by 61% of the imposed lateral displacements compared to 24% recovery by SW-S(R).
5. The SMA wall provided a 19.7% greater secant stiffness than SW-S(R) at 2.5% drift.

Acknowledgements

The authors would like to acknowledge Mansteel; CRH – Dufferin Concrete; and Sika Canada for their generous donations of materials.

References

Abdulridha, Alaa. 2013. Performance of Superelastic Shape Memory Alloy Reinforced Concrete Elements Subjected to Monotonic and Cyclic Loading. *Ph.D. Thesis*, University of Ottawa, 1-346.

Abdulridha, A., and Palermo, D. 2017. Behaviour and Modelling of Hybrid SMA-steel Reinforced Concrete Slender Shear Wall. *Engineering Structures*, Elsevier, **147**(2017): 77-89.

Abdulridha, A., Palermo, D., Foo, S., and Vecchio, F. J. 2012. Behaviour and Modelling of Superelastic Shape Memory Alloy Reinforced Concrete Beams. *Engineering Structures*, Elsevier, **49**(13): 893-904.

Alam, M. S., Nehdi, M., and Youssef, M. A. 2007. Applications of Shape Memory Alloys in Earthquake Engineering. Ninth Canadian Conference on Earthquake Engineering, 1468-1477.

ATC-24. 1992. Guidelines for Cyclic Seismic Testing of Components of Steel Structures. AISI.

CSA A23.3-04. 2004. Design of Concrete Structures. Canadian Standards Association. Rexdale, Canada.

Menna, C., Auricchio, F., and Asprone, D. 2015. Applications of Shape Memory Alloys in Structural Engineering. *Shape Memory Alloy Engineering*, Elsevier, **109**(2): 369-403.

Ozbulut, O. E., Hurlebaus, S., and DeRoches, R. 1983. Drained Axisymmetric Loading of Reinforced Clay. *Journal of Geotechnical Engineering*, ASCE, **109**(2): 883-898.

Park, R. 1989. Evaluation of Ductility of Structures and Structural Assemblages From Laboratory Testing. *Bulletin of The New Zealand National Society for Earthquake Engineering*, **22**(3): 155-166.

Ramirez, C. M., and Miranda, E. 2012. Significance of Residual Drift in Building Earthquake Loss Estimation. *Earthquake Engineering and Structural Dynamics*, IAEE, **41**(2012): 1477-1493.

Saiidi, M., and Wang, H. 2006. Exploratory Study of Seismic Response of Concrete Columns with Shape Memory Alloys Reinforcement. Structural Journal, ACI: 436-443.

Yazgan, U. 2010. The Use of Post-Earthquake Residual Displacement as a Performance Indicator in Seismic Assessment. *IBK Bericht*, ETH Zurich, **330**(2010): 1-232.